SLAC-J-ICFA-16
July 1998
SLAC-R-647

HOME PAGE

http://www.slac.stanford.edu/pubs/icfa/

ICFA INSTRUMENTATION BULLETIN*

The publication of the ICFA Instrumentation Bulletin is an activity of the Panel on Future Innovation and Development of ICFA (International Committee for Future Accelerators).

Volume 16

. Summer 1998 Issue

* Supported by the Department of Energy, contract DE-AC03-76SF00515.

ICFA INSTRUMENTATION BULLETIN

The publication of the ICFA Instrumentation Bulletin is an activity of the Panel on Future Innovation and Development of ICFA (International Committee for Future Accelerators). The Bulletin reports on research and progress in the field of instrumentation with emphasis on application in the field of high-energy physics. It encourages issues of generic instrumentation.

Publisher : Stanford Linear Accelerator Center
SLAC Publications Department
Stanford, CA 94309, U.S.A.

Editor : J. Va'vra

Web Technical Advisers : J. Schwiening and T. Pavel

Cover: The illustration depicts L. J. Waghenaer's marine atlas, "The Mariner's Mirror," published in 1588. Lucas Janszoon Waghenaer was born in Holland in the 1530s. He became a famous ship pilot in his time. In 1584, he published the atlas ("Spieghel der Zeevaerdt") which was greatly valued among mariners for centuries. This was not due only to the map content, but also to the detailed knowledge of navigation techniques of that time. The atlas, as it appears on our page, is the same one used for the Dutch to English translation.

Table of Contents

1998 Conference List

- The 6-th International Conference on Advanced Technology and Particle Physics, Vila Olmo, Como, Italy, October 5-9, 1998.
- IEEE Nucl. Sci. Symposium, Toronto, Canada, November 5-9, 1998.
- The 3-rd International Workshop on Ring Imaging Cherenkov Detectors (RICH'98) Ein-Gedi, Dead-Sea, Israel, November 15-20, 1998.

98-08-105

A NEW TYPE OF SPARK-PROTECTED PARALLEL MESH CHAMBER

P. Fonte[1,2], N. Carolino[1], L. Costa[3], R. Ferreira-Marques[1,4], S. Mendiratta[3], V. Peskov[5], A. Policarpo[1,4]

1-LIP, Dep. de Fisica, Univ. de Coimbra, 3000 Coimbra, Portugal.
2-ISEC, Quinta da Nora, 3000 Coimbra, Portugal.
3-Departamento de Fisica, Univ. de Aveiro, 3800 Aveiro, Portugal.
4-Departamento de Fisica, Univ. de Coimbra, 3000 Coimbra, Portugal.
5-NASA Marshall Space Flight Center, Huntsville, AL 35812, USA.

ABSTRACT

We developed a very low resistivity RPC-type detector, the anode of which was a plate made from materials with resistivity up to $5x10^7$ Ωcm, the cathode being a metallic mesh preceded by a drift region.

In such a detector it was actually possible to combine the versatility and high counting-rate capability of metallic PPACs with the extreme robustness and "protectiveness" of Resistive Plate Chambers.

Occasional discharges triggered by large deposits of primary ionization or by extreme counting rates are quenched by the resistive anode and are constrained to the glow discharge phase of the sparking process. The study shows that this discharge affects the detector only locally and the charge released is limited to a few tens of nC.

Proportional counting rates of up to 10^5 Hz/mm^2 were achieved at gains above 10^4. The energy resolution at 6 keV was 20% FWHM. The observed gain-rate trade-off is well-described by an analytic model, and further improvements may be expected by lowering the resistivity of the anode material.

The properties of several custom-made, controllable resistivity, anode materials are described and perspectives of improvement in the performance of the detector are discussed.

1. Introduction

Parallel geometry chambers are used in three main configurations: Parallel Plate Chambers (PPCs), with two metallic electrodes. Resistive Plate Chambers (RPCs) with two resistive electrodes and Parallel Mesh Chambers[1] (PMCs) with multiple wire-mesh electrodes [1].

Common features of these detectors when operated in proportional mode, are the good timing characteristics [2], good position resolution [3], and easiness of production in large areas and large gain. The maximum gain is limited to the point where individual avalanches reach a charge around 10^8 electrons, triggering the formation of streamers [4] that subsequently evolve to higher current discharges [5]. Recently, a new rate-induced breakdown mode was identified in PMCs [6].

In chambers with metallic electrodes (PPCs, PMCs) the discharge progresses until fully formed sparks appear. Although the sparks don't seem to affect the detector in a permanent way [7], the phenomenon causes unacceptable dead times and may compromise the integrity of the readout electronics.

When the electrodes are highly resistive (RPCs), the discharge is quenched at an earlier stage, affecting the detector only locally and being harmless to the readout electronics. It is even possible to operate the RPCs in a saturated gain "streamer mode," featuring very large and fast signals, up to a few hundred pC [8].

The advantage of RPCs in terms of sparkless operation is offset by a severe counting rate limitation of a few tens of Hz/mm^2, while PPCs and PMCs can reach counting rates at least up to 10^5Hz/mm^2 [6,9] without any decrease of the pulse-height, suggesting their use as high-rate detectors.

It is attractive to attempt to combine the "protectiveness" of RPCs with the large counting rate capability of the metallic chambers. Earlier attempts [10] were focused on an asymmetric RPC with wire-mesh electrodes, except for a resistive anode made of Pestov glass. However, due to a lack of anode materials with lower resistivity, the counting rate of the device didn't exceed a few hundreds of Hz/mm^2.

In the present work, we introduce a new custom-made medium resistivity material whose resistivity can be controlled from $2x10^7$ to $3x10^{12}$ Ωcm allowing for a large flexibility in the chamber counting characteristics, while keeping essentially the same hybrid configuration described above.

The resulting detector actually combines the high counting-rate capability of PMCs (10^5Hz/mm^2), while keeping the extreme robustness and "protectiveness" of RPCs.

[1] Also known historically as Parallel Plate Avalanche Chambers (PPACs), although in these detectors there are no plate electrodes.

2. Experimental Setup

A schematic drawing of the experimental set-up can be seen in Fig.1. The detector was constituted by a drift region followed by an amplifying gap. The drift region was 15 mm long and delimited by two wire meshes. The amplifying gap, 3.5 mm long, was delimited by the lower drift mesh (cathode) and by a resistive plate (anode). The meshes were made of stainless steel wires of 50 mm diameter placed at a pitch of 0.5 mm. The detector had an active diameter of 4 cm.

The primary charges were created by a collimated X-ray beam produced by a sharp-focus (0.1 mm) X-ray tube having a Fe anode. The tube produces a Bremsstrahlung photon energy distribution peaked at 5.5 keV, with a maximum energy of 10 keV. The beam was filtered by a nickel foil to absorb the lowest energy photons and delimited by a flat ring collimator placed 4 cm from the tube anode, with selectable openings of 2 and 5mm diameter. The collimator was placed over the Mylar entrance window, 1 mm from the upper drift mesh. It is estimated that the 5.5 keV photons will generate 200 primary electrons, and this was the value used for all calculations.

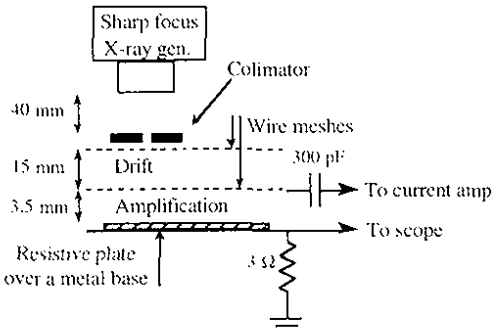

Figure 1. Schematic representation of the experimental setup.

The resistive plate was deposited over a flat metal plate that provided mechanical support and a uniform electrical connection to the plate. The metal plate was grounded through a 3 Ω resistor, and the current signal from discharges could be recorded directly on a scope connected in parallel with the grounding resistor.

The cathode signal was read out through a capacitor by a current amplifier with a 30 ns risetime. Since the rise time of the amplifier was actually longer than the signal width, the pulse height at the amplifier output was related to the avalanche charge and not to the gap current. It was found that the observed pulse shape at the amplifier output was well reproduced by injecting in parallel with the amplifying gap a square current pulse of 10 ns width. When the amplitude was

160 mA, this pulse corresponded to the injection of 10^7 electrons or 1.6 pC, thus providing a charge calibration of the readout system.

In order to measure the overall counting rate, the output of the fast current amplifier was sensed by a discriminator whose trigger rate was measured by a time-windowed scaler. The peak noise level at the amplifier output was around 25 fC, and the discriminating threshold for all measurements was placed at 80 fC. This relatively high level was forced by a noisy X-ray tube power supply.

If the resistive plate is considered in first approximation to be a purely ohmic conductor, a simple equivalent electrical circuit from the signal-source point of view can be derived (Fig. 2). It can be calculated that the gap capacity per unit area is $C_{gap}=0.25pF/cm^2$ and that the plate capacity per unit area is around $C_{plate}=2.6pF/cm^2$ (assuming $\epsilon_r=3$ and a plate thickness of 1mm). The total capacities can be estimated by multiplying those values by the plate area of 25 cm^2. The value of the readout capacitor is $C_{readout}=300pF$.

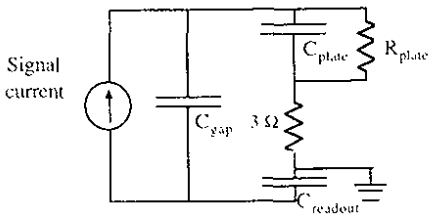

Figure 2 Equivalent electrical circuit from the signal source (avalanche or streamer) point of view.

The gas mixture was constituted by Ar+20%C_2H_6 + methanol. The mixture was 50% saturated with the methanol vapors, that were required to prevent the resistive plate from becoming dry, with a consequent increase of the plate surface resistivity.

3. Resistive material

The anodic resistive plate was made from a mixture of epoxy[2] and ink[3], that yields a black rubber-like material.

[2] Araldite.

[3] MOLIN, ball-point pen black ink.

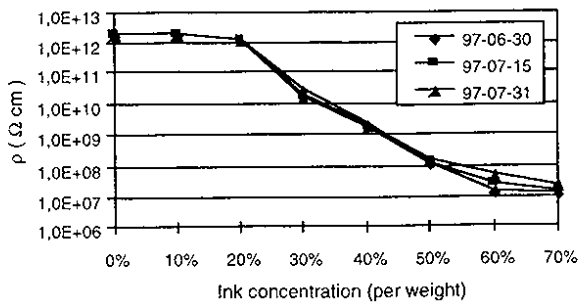

Figure 3. The anodic material resistivity can be controlled by the amount of ink and varied from $2x10^7$ to $3x10^{12}\Omega$cm. Successive measurements taken at two-week intervals suggest a good stability of the bulk resistivity.

The resistivity can be varied from $2x10^7$ to $3x10^{12}\Omega$cm by varying the ink concentration (Fig. 3). Successive measurements taken at two-week intervals suggest a good stability of the bulk resistivity.

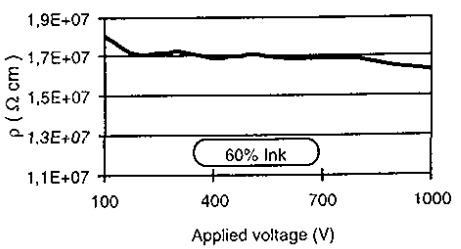

Figure 4. The resistivity is largely independent from the applied voltage, indicating an ohmic behavior.

The material shows an ohmic behavior up to an applied voltage of 1kV (Fig. 4), and although there is some relaxation effect, the short-term histeresis cycle is quite narrow (Fig. 5).

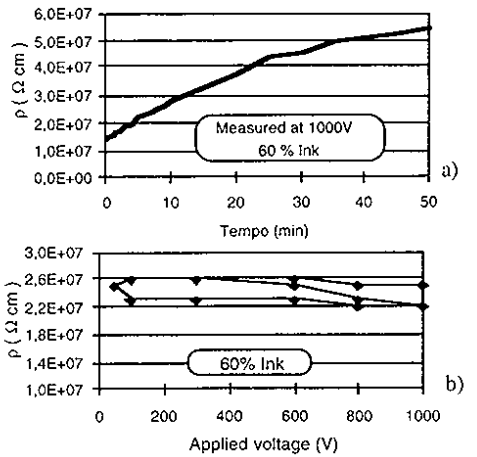

Figure 5. Although the material shows a marked relaxation effect with a characteristic time of about 30 minutes (a), the fast cycling (1 minute per point) through large voltage excursions results in a relatively narrow histeresis plot (b).

Further measurements have been performed in a systematic way, trying to identify materials of potential interest for this type of application. In particular, Fig. 6 shows results for melamine and for the above material, together with ABS plastic doped with $FeCl_3$. The later seems to be a promising candidate, having much better mechanical characteristics than the epoxy-ink mixture. It is interesting to note the marked dependence of the resistivity with temperature.

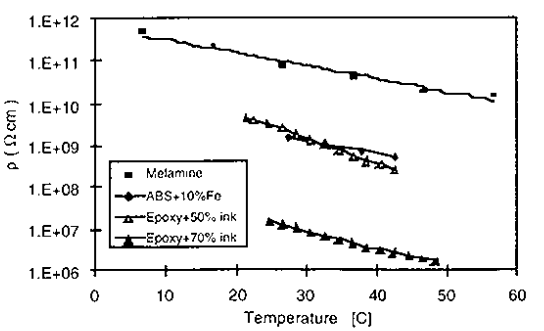

Figure 6. Resistivity measurements performed for various materials in a temperature range of practical interest.

4. Results and Discussion

4.1 Counting Characteristics

The detector shows a reasonable energy resolution of 20% FWHM (Fig. 7) for 5.9 keV X-rays, while the best results for PMCs are typically around 14% FWHM [11]. In principle, there is no reason why the present detector cannot achieve similar resolution values, so we attribute the observed reduced resolution to the deficient parallelism of the gap and to edge effects arising from the relatively small diameter of the active area.

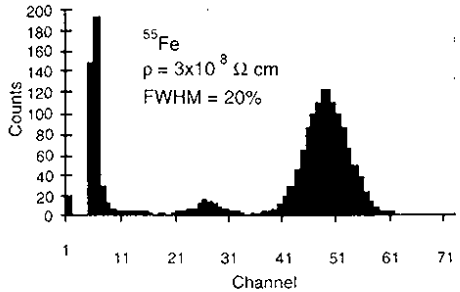

Figure 7. A 20% FWHM energy resolution was observed when the detector was illuminated by a ^{55}Fe radioactive source emitting 5.9 keV X-rays.

A large counting plateau of more than one order of magnitude in gain was observed when the detector was illuminated by 5.9 keV X-rays (Fig. 8). The corresponding dark current is negligible and sparks appear only at gains in excess of 10^6. The dark current was found to be extremely sensitive to the presence of dust particles, requiring the detector to be assembled in a dust-free environment.

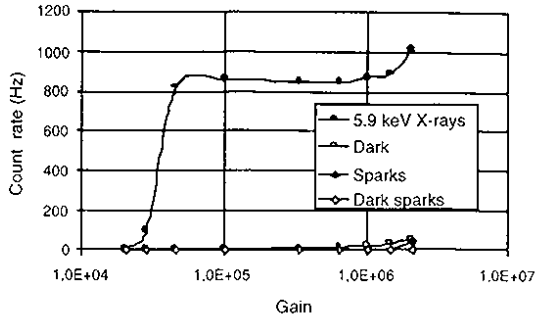

Figure 8. A large counting plateau of more than one order of magnitude in gain was observed when the detector was illuminated by 5.9 keV X-rays. The corresponding dark current is negligible and discharges appear only at gains in excess of 10^6.

The gain-rate characteristics of the detector were studied for several combinations of applied voltages, plate materials and beam diameters, the detector being illuminated with X photons generated by the tube described in section 2. The results are shown in Fig. 9.

For all plate materials, with resistivity ranging from $4x10^7$ Ωcm to $4x10^{11}$ Ωcm, a reduction in gain for fixed applied voltage was observed above a certain rate threshold. The threshold rate is different for each plate, but seems to be relatively unaffected by the operating voltage or by the beam diameter.

For the lower plate resistivity studied, counting rates of 10^5Hz/mm^2 were achieved at gains between 10^4 and 10^5. This value is actually slightly above the intrinsic rate-gain limitations that were found in similarly built metallic PMCs [6], indicating that the optimum anode resistivity has been reached. The fact that in RPCs one can reach higher gains than in metallic chambers is well established in the literature, probably due to the "protectiveness" provided by the resistive electrodes.

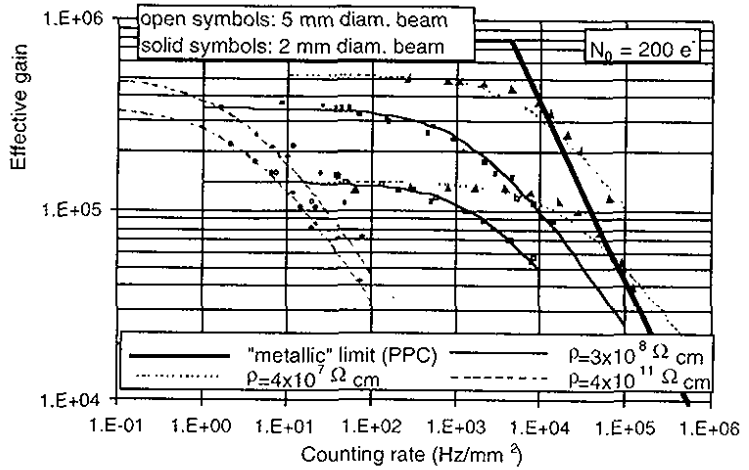

Figure 9. Gain-rate characteristics of the detector for several values of the anode plate resistivity, beam diameters of 2 and 5 mm and two values of the applied voltage for each plate. For the lower resistivity case, counting rates of 10^5Hz/mm^2 were achieved at gains between 10^4 and 10^5. The thin lines were adjusted according to the model described in the text, and the thick solid line marks the experimentally determined intrinsic counting rate limitations of a similarly built all-metallic PMC [6].

4.2 *A Model of the Rate-Gain Dependence*

The simplest assumption one can make about the origin of the rate-gain dependence is that it is caused by a reduction of the effective gap electric field owing to an ohmic voltage drop across the anode plate when crossed by the average avalanche current.

Mathematically, the model can be expressed by the equations:

$$V = V_0 - R\, I(V)\,,$$

$$R = \rho\frac{L}{S} \qquad I(V) = f\, e\, N_0\, G(V)\,,$$

$$\frac{\ln G(V)}{d} = A\exp\left(-\frac{B}{E}\right), \qquad E = \frac{V}{d}\,, \qquad (1)$$

where V is the effective voltage across the gap, V_0 is the applied voltage, $I(V)$ is the gap current, R is the resistance seen by the gap current, r is the plate resistivity, L is the plate thickness, S is the beam cross section, f is the counting rate, e N_0 is the primary charge, $G(V)$ is the effective gain written in the Korff approximation, and d is the gap length. The parameters A and B were determined experimentally for the gas mixture used.

The model relates the effective gap voltage V (as an implicit function) to the other quantities. Since the plate resistivity under the actual operating conditions is the most uncertain parameter of the model (actually immeasurable directly), it was chosen as a free parameter to be adjusted to the data.

The predicted rate-gain dependence was plotted in Fig. 9 (thin lines). It can be seen that the model describes reasonably well the observed behavior. Additionally, in Table 1 the adjusted values of the plate resistivity are shown for each curve and compared to the externally measured DC resistivity. The values agree within a factor of two, seeming to validate the model when we consider that the range of resistivities covers four orders of magnitude and that the model doesn't take into account the beam-edge effects or the non-ohmic behavior of the material.

	Externally measured	Adjusted V_{01}	Adjusted V_{02}
r (Ωcm)	4.0×10^{7}	5.8×10^{7}	3.8×10^{7}
	3.8×10^{8}	3.5×10^{8}	1.8×10^{8}
	4.1×10^{11}	8.7×10^{11}	6.1×10^{11}

Table 1 - Comparison between the values of the plate resistivity (r) measured externally and the values estimated from the model after a least-squares fit to the data points shown in figure 9 (V_{01} and V_{02} refer to the values of the applied voltage used for each plate). The resistivity values agree within a factor of two, seeming to validate the model.

4.3 *Streamer charge*

Discharges were triggered by streamers when the gain exceeded 10^6, that is, when the avalanche charge exceeded 2×10^8 electrons. Eventually, some of the highest rate points shown in Fig. 9 correspond to the limit of rate-induced breakdown [6], but this was not directly verified experimentally.

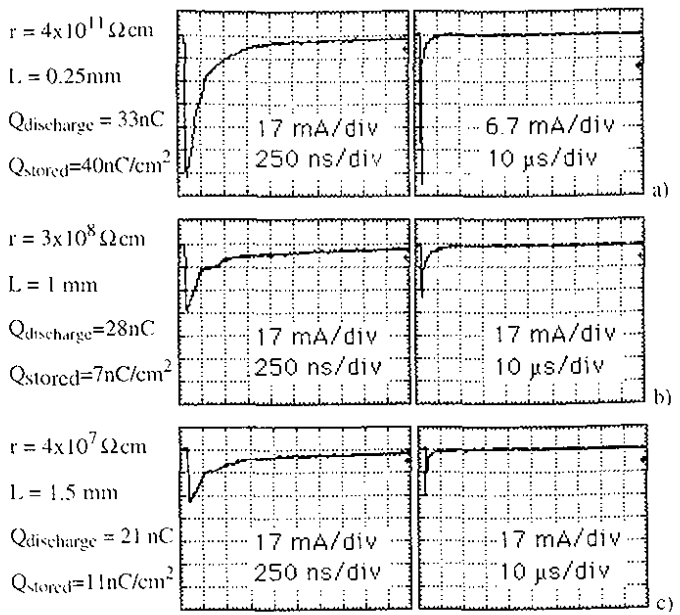

Figure 10 - Typical oscilograms of the discharge current for the anode plates studied in two different time scales. The quantities listed to the left of the oscilograms are: plate DC resistivity (r), plate thickness (L), observed discharge charge ($Q_{discharge}$), and charge stored in the plate capacitor per unit area (Q_{stored}).

As described in section 2, the discharge current could be observed directly on an oscilloscope, with typical waveforms shown in Fig. 10. The characteristics listed to the left of the waveform are: plate DC resistivity (r), plate thickness (L), observed discharge charge ($Q_{discharge}$), and charge stored in the plate capacitor per unit area (Q_{stored}). The discharge charge was estimated by integrating the area under the leftmost waveform for each plate and Q_{stored} was calculated from C_{plate} (see section 2) assuming a typical applied voltage of 4 kV. From the values given in section 2, one can conclude that $C_{readout} >> C_{plate} >> C_{gap}$ and from Fig. 2 it can be seen that, from the capacitive point of view, the ratio between the charge transferred across the gap and the corresponding voltage change is dominated by C_{plate}.

For Fig. 10a, ($r=4x10^{11}\ \Omega cm$), $Q_{discharge}$ is lower than Q_{stored}, corresponding to the release of the charge stored in a fraction of a cm^2 of the plate surface.

For Fig. 10b and c, $Q_{discharge}$ is larger than Q_{stored} by a factor two to three, suggesting that the conduction of current across the plate during the duration of the discharge is able to feed the discharge with an amount of charge at least comparable to the charge released from the plate surface.

Interestingly, the contribution to $Q_{discharge}$ from conduction across the plate is not proportional to the measured DC plate resistivity (r). This may be attributed to the fact that the discharge occurs in a short time (1 ms), corresponding to a high-frequency voltage pulse applied to the plate, whose high-frequency resistivity may be completely different from the DC value.

4.4 *Type of Discharge*

According to Ref. 5 the development of violent sparks in parallel geometry is preceded by a sequence of intermediate stages comprising the following discharge types: avalanche, streamer, glow discharge, filamentary discharge, and spark.

In the present case the discharges were visually identified as being of the glow-discharge type, featuring a bright cathode spot at the apex of a faint conic-shaped glow region that extends up to the anode. It seems that the current restriction imposed by the anode material prevented the process to evolve beyond the glow-discharge stage.

For the lower resistivity material ($r=4x10^7\ \Omega cm$), sometimes the glow discharge would be unquenched, fed by the conduction current across the plate. An increase in the amount of quencher (C_2H_6) in the gas mixture strongly reduced the frequency of this phenomenon, without completely avoiding it. However it seems probable that the use of more efficient quenchers like isobutane or DME would further alleviate the problem.

5. Conclusions

We built and tested an asymmetric Resistive Plate Chamber able to achieve proportional counting rates up to 10^5 Hz/mm^2 at gains between 10^4 and 10^5. The energy resolution at 5.9 keV was 20% FWHM.

The chamber was constituted by an amplifying gap delimited by a resistive plate anode and a wire mesh cathode, preceded by a drift region. A new custom-made medium resistivity material was used for the anode plate, whose resistivity could be controlled from $2x10^7$ to $3x10^{12}\ \Omega$cm.

Eventual discharges were quenched by the current limitation imposed by the resistive anode and constrained to the glow discharge phase of the sparking process. The discharge affected the detector only locally and the charge released was limited to a few tens of nC, independently of the plate DC resistivity.

The observed gain-rate tradeoff is well described by a simple ohmic model.

Being the characteristic relaxation time of an anodic plate (*re*) of the order of a few ms, the electric transparency of the anode plate is preserved for the fast (<100 ns) electron signal. This will, in principle, allow a two-dimensional strip readout to be placed below the anodic plate, with typical position resolutions of 100 to 200 mm [3].

Finally, the spark protection concept presented here may also be useful when applied to higher-rate detectors like MICROMEGAS or other thin-gap parallel geometry chambers [12]. In such a case, lower resistivity materials will be required and further research is therefore needed.

6. Acknowledgments

The authors gratefully acknowledge Crispin Williams and the LAA Project for lending some of the necessary hardware.

This work was done in the framework of the projects JNICT-CERN/P/FAE/1098/96 and JNICT-CERN/P/FAE/1143/97.

7. References

[1] G. Charpak and F. Sauli, *Phys. Lett.*.B, 78 (1978) 523.

[2] E. Ceron Zebalos, *Sci. Acta* XI-1, (1996) 317.
A. Arefiev et al., *Sci. Acta* XI-1, (1996) 359.
M. Angelone et al., *Nucl. Instrum. Meth.* A355 (1995) 359.

[3] A. Peisert et al., *Nucl. Instrum. Meth.* A247, (1986) 435.
E. Ceron Zebalos, *Nucl. Instrum. Meth.* A392, (1997) 150.

[4] H. Raether, *Electron Avalanches and Breakdown in Gases* (London, Butterworths, 1964).
J.M. Meek, in *Electrical Breakdown of Gases*, ed. J.A.Rees (London, MacMillan, 1973).
P. Fonte et al., *Nucl. Instrum. Meth.* A310, (1991) 140.
P. Fonte, *IEEE Trans. Nucl. Sci.* vol.43, (1996) 2135.

[5] S.C. Haydon, in *Electrical Breakdown of Gases*, ed. J.A. Rees (London, MacMillan, 1973).

[6] Y. Ivaniouchenkov et al., "*The high rate behaviour of Parallel Mesh Chambers,*" presented at the 1997 IEEE Nuclear Science Symposium, 9-15 November, Albuquerque, New Mexico, USA, to be published in IEEE Transactions in Nuclear Science.

[7] A. Arefiev et al., *Sci. Acta* XI-1, (1996) 359.

[8] I. Duerdoth et al., *Nucl. Instrum. Meth.* A348, (1994) 303.
R. Cardarelli et al., *Sci. Acta* XI-1,(1996) 11.
P. Fonte, *Sci. Acta* XI-1, (1996) 25.

[9] A. Peisert, *Nucl. Instrum. Meth.* 217, (1983) 229.
J. Hendrix et al., *Nucl. Instrum. Meth.* A252, (1986) 246.

[10] V. Peskov et al., FERMILAB TM-1838, 1993
D.F. Anderson et al., *Nucl. Instrum. Meth.* A348, (1994) 324.

[11] B.D.Ramsey et al., *Nucl. Instrum. Meth.* A248, (1986) 550.

[12] Y. Giomataris, *Nucl. Instrum. Meth.*, A376, (1996) 29.
P. Fonte et al., "*Thin gap parallel mesh chamber: a sparkless high-rate detector,*" preprint LIP/97-05, December 1997 (http://xxx.lanl.gov/abs/physics/9803021).

98-08-106

WHICH GASEOUS DETECTOR IS THE BEST AT HIGH RATES?

P. Fonte[1], V. Peskov[2], and B.D. Ramsey[2]
[1]LIP, Coimbra University and ISEC, Coimbra, Portugal
[2]NASA/Marshall Space Flight Center, Al 35812, USA

Abstract

We report results from a systematic study of breakdown limits for various high rate gaseous detectors: PPAC's, MGC's, diamond-coated MSGC's, MICROMEGAS and CAT. It was found that for all these detectors, the maximum achievable gain, before breakdown appears, drops dramatically with incident flux and is sometimes inversely proportional to it. Further, in the presence of alpha particles, typical of the backgrounds in high-energy experiments, additional gain drops by one or two orders of magnitude were observed for some detectors. We discovered that breakdowns at high rates occur through what we have termed an "accumulative mechanism," which does not seem to have been previously reported in the literature. Results of these studies may help to choose the optimum detector for given experimental conditions.

1. Introduction

Future high-luminosity experiments make serious demands on detector technologies and have prompted a chain of inventions of new high-rate gaseous detectors: MSGC's[1], MGC's[2], CAT[3], MICROMEGAS[4], and GEM [5]. Due to the extremely tight time scales involved, some of these detectors were almost immediately adopted for the large experiments at CERN and elsewhere. The aim of this work is to perform an independent systematic study of the breakdown limits of these and other gaseous detectors recently chosen or considered as candidates for high-luminosity applications.

2. Experimental set-up

The experimental set-up was described in detail in Ref. 6 and is presented schematically in Fig. 1. It consists, in essence, of a test chamber inside of which the various detectors under study were installed. We investigated the rate behavior of the following detectors: PPAC's, MGC's, diamond-coated MSGC's, thin-gap PPAC's, CAT, and MICROMEGAS. The detailed description of their designs are given in Refs. 6 and 7. In some measurements a MWPC was also used. This device had 20-micron anodes on a 3-mm pitch with a 4-mm gap between cathode planes, the lower of which was a solid metallic sheet and the upper was an 80% transparent mesh with a drift space above if necessary. Additional studies were done combining all the above devices with preamplification structures: GEM, PPAC, or MICROMEGAS-type [6,8]. Most of the measurements were done in Ar-based mixtures at pressure of 1 atm, although other mixtures and

pressures were occasionally tested [6]. As sources of primary ionization, we used an X-ray gun with variable photon energies (6, 17, or 30 keV), and alpha particles collimated perpendicular to the detector surfaces. The full procedures for gain calibration and the measurements of breakdown limits are described in Refs. 6 and 9.

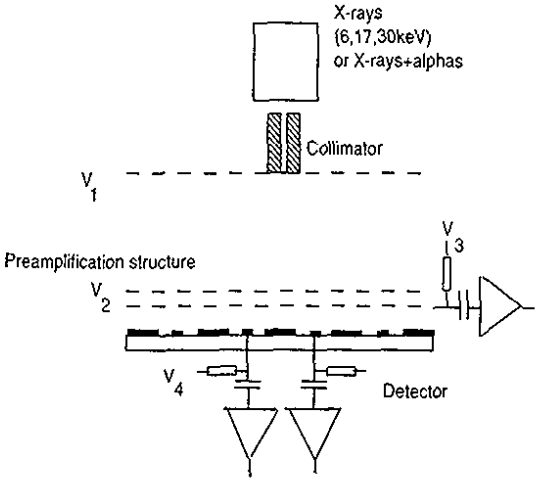

Fig. 1. Schematic drawing of the experimental set-up.

3. Results

The main results of our studies are summarized in Figs. 2 and 3. In Fig. 2 we plot the maximum achievable gain before the breakdown appears under irradiation with 6 keV x-rays. As one can clearly see, for all detectors tested the maximum achievable gain drops with rate. The highest gains were obtained with MSGC's with preamplification structures [6] , MICROMEGAS [10], and thin gap PPAC's [9]. It is interesting to note that the use of any preamplification structure for MICROMEGAS, PPAC's did not give any significant increase of the total gain [6, 9]. This is thought to be due to charge-cloud expansion in the preamplification structure which has dramatic effect on the confined avalanche of the MSGC, but a much smaller effect on the broader parallel-plate-type avalanche of MICROMEGAS and PPAC's (see Ref. 8 for more details). During these studies we discovered an interesting feature of the MICROMEGAS and thin gap PPAC detectors: the discharge which appears at breakdown is self-quenched, that is, the energy released in the spark is much less than that stored by the detector's capacitance [9]. Our measurements also show

that the energy released in the spark is much less than in conventional PPAC's which have even lower capacitance. This feature makes them unique for many applications.

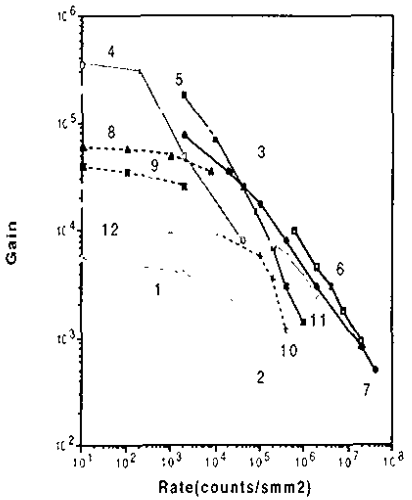

Fig. 2. The maximum achievable gain (curves 1-7), as a function of X-ray flux, for various detectors: (1) diamond-coated MSGC with 0.2 mm pitch, (2) diamond-coated MSGC with 1-mm pitch, (3) MSGC (1) combined with GEM, (4) MSGC (2) combined with GEM, (5) PPAC with 3-mm gap, (6) MICROMEGAS [10], (7) thin gap (0.6mm) PPAC [9], (8-12) space-charge gain limit as a function of rate for the MWPC: (8-10) replotted from Refs. [12-14], (11) thin gap MWPC [14]. In the case of 11 and 12, the value of gas gain is estimated from data given in [14]. (12) our measurements for MWPC. The curve for CAT is close to that of curve 1 and so is not plotted to simplify the figure.

One should note that the absolute value of the maximum achievable gain before breakdown occurs depends, of course, on the gas mixture and this may give a powerful parameter for detector optimization. However, the tendency is that for all mixtures tested, the maximum achievable gain drops with rate. The maximum achievable gains for the MGC and MSGC never exceed $2x10^4$ [11] and for MICROMEGAS, $2x10^5$ [10], even with optimized gas mixtures. When combined with preamplification structures, however, the MSGC in an (MSGC+GEM) configuration gave gains of $2x10^5$-10^6 in all gas mixtures tested, which made it superior to all other devices.

For comparison, Fig. 2 also shows data for conventional and thin-gap MWPC's [12,13,14]. In these cases, the high counting rate does not trigger any breakdowns, but lowers the amplitudes due to an accumulation of space charge. Therefore, Fig. 2 does not show the maximum gain, but

the changes in amplitudes due to the space charge effect. It is perhaps surprising to see that these detectors have reasonable rate capabilities too.

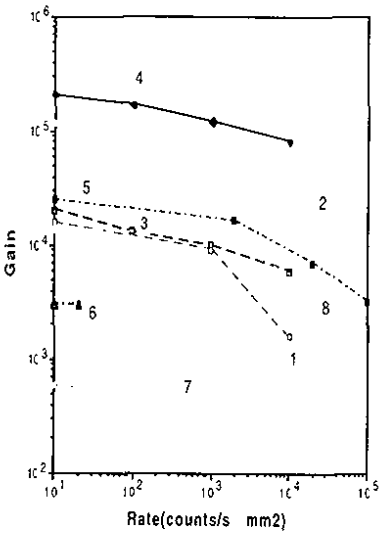

Fig. 3. Maximum achievable gain (curves 1-7) as a function of x-ray flux in the presence of alphas for:

(1) diamond-coated MSGC with 1 mm pitch , (2) MSGC (1) with GEM, (3) diamond-coated MSGC with 0.2 mm pitch (from Ref. [15]), (4) MSGC (2) with GEM, (5) PPAC with 3 mm gap, (6) thin gap (0.6 mm) PPAC, (7) CAT, (8) space-charge-limited gain variation for the MWPC in the presence of alphas at counting rate <100 Hz per 1cm of wire (our measurements).

Figure 3 shows the results under identical x-ray irradiating conditions to those in Fig. 2, but with the addition of a collimated beam of alpha particles at a few kHz per few mm^2. In this case for the PPAC-type of detectors (PPAC, thin gap PPAC, and CAT), an additional drop on one or two orders of magnitude (depending on the energy deposit in the drift gap) was observed. In this environment, the highest gains were achieved with the MSGC combined with a preamplification structure [6]. As an independent confirmation, we also plot in Fig. 2 data from the Sauli group [15].

Finally, it is interesting to note that we found that the dependence of gain variation with a rate of x-photons for the MWPC remains almost constant if the rate of the alpha particles was <100 Hz. Therefore, the MWPC still remains attractive for many applications.

4. Discussion

We discovered that the maximum achievable gain in *ALL* the gaseous detectors tested drops dramatically, in some cases inversely proportional, with count rate. Further, in the presence of alpha particles, typical of the backgrounds in high-energy experiments, additional gain drops one or two orders of magnitude may appear. These measurements permit clear recommendations for choosing the optimum detector for particular experimental conditions. For example, for measurements of strong x-ray radiation (synchrotron radiation), MSGC+GEM, MICROMEGAS, and thin-gap PPAC's will be ideal candidates. However, in the presence of alphas a good choice would be the MSGC with a preamplification structure, or even a conventional or thin-gap MWPC if their spatial resolution can satisfy the user's requirements. The MWPC can operate at high gains(A) in the presence of alphas as its total charge is not the critical parameter for corona-type breakdown, only its gain, which must remain below A*g = 1, where g is a probability of secondary processes. Of course, MICROMEGAS, CAT, and thin gap PPAC still can operate at relatively high gains in the presence of alphas, but in this case the drift space should be reduced to 1 mm or less to limit the primary charge.

It is interesting to note that rate-limiting breakdowns in most of the high rate detectors do not occur through any of the three standard breakdown mechanisms invoked at low rates (streamers or two types of feedback loops)[16]. For example, in PPAC-type detectors (PPAC, MICROMEGAS, thin gap PPAC), high-incident-flux breakdowns occur through a memory effect: that is, the discharge gap somehow remembers the previous avalanche (for time intervals often much longer than the removal time of the ions!) and this lowers the breakdown limit. We call this new breakdown mechanism an accumulative breakdown, which may be associated with several phenomena. The most important of these is the ejection of jets of electrons by ion bombardment of exposed cathode surfaces, which can continue for minutes beyond the actual bombardment. Another is associated with the accumulation of excited atoms in the avalanche region, which may reach a critical concentration and provoke discharges. This latter phenomena was observed in pure noble gases [17] and there is speculation that this may also be responsible for streamer formation in the mixtures of gases [18]. The results of a detailed study of this type of breakdown are given in Ref. 19.

Conclusion

The highest achievable gain for x-rays (and presumably for minimum ionizing particles) are achievable in MSGC+GEM , MICROMEGAS, and thin gap PPAC's. However, in the presence of heavy ionizing particles, MSGC+GEM can offer higher gains. In some high-rate measurements, the standard or thin-gap MWPC can also be used if its spatial resolution satisfies requirements.

Acknowledgments

We thanks G. Charpak, F. Sauli , A. Policarpo, R. Bellazzini and Y. Giomataris for useful discussions.

References

[1] A. Oed, Nucl. Instr. and Meth., A263 (1988) 351.

[2] F. Angelini et al., Nucl. Instr. and Meth., A335 (1993) 69.

[3] F. Bartol et al., French J. Phys., 6 (1996) 337.

[4] Y. Giomataris et al., Nucl. Instr. and Meth., A376 (1996) 29.

[5] F. Sauli, Nucl. Instr. and Meth., A386 (1997) 531.

[6] P. Fonte et al., "Rate and gain limitations of MSGC's and MGC's combined with GEM or other preamplification structures," NASA preprint, submitted to the Proceedings of the Vienna Wire Chamber Conference, February 1998.

[7] P.Fonte et al., "Breakdown features of various microstrip-type gas counter designs and their improvements," to be published in the Proceedings of IEEE Nucl. Sci. Sympos., Alberquerque, USA, 1997.

[8] P. Fonte et al., "A study of breakdown limits in microstrip gas counters with preamplification structures," submitted to Nucl. Instr. and Meth., 1997

[9] P. Fonte et. al. "Thin gap parallel-mesh chamber: a spark-less high-rate detector," Preprint LIP 97-05, 1997

[10] Y. Giomataris private communication, March 1998.

[11] B. Bomska et al., "Investigation of discharge limits in diamond-coated microstrip gas chamber," CERN-PPE-GDD, 1996.

[12] A. Breskin et al., Nucl. Instr. and Meth., 124 (1995) 189.

[13] A.H. Walenta, Physica Scripta, 23 (1981) 354.

[14] R.A. Levis et al., Nucl. Instr. and Meth., A 392 (1997) 42.

[15] R. Bouclier et al., Nucl. Instr. and Meth., A396 (1997) 50.

[16] H. Raether, "Electron avalanches and breakdowns in gases", Butterworth, Washington 1964.

[17] V. Peskov, Sov. Phys. Tech. Phys., 20 (1976) 1584.

[18] L.S. Zhang, Nucl. Instr. and Meth., 247 (1986) 343.

[19] P. Fonte et al., "Fundamental gain limitations of gaseous detectors and optimum designs for high-rate applications," a report submitted to the IEEE-98 Nucl. Science Symp.,1998.

PP-08-107

Properties of some gas mixtures used in tracking detectors

Archana Sharma
GSI-Darmstadt, Germany*

Abstract

This report summarizes some useful data on the transport characteristics of gas mixtures which are required for detection of charged particles in gas detectors. The requirements for high luminosity tracking are stringent and different at low and high momenta, representing a compromise between a fast gas mixture, small diffusion properties, and having a small Lorentz angle, but high primary ionization. With the advent of a host of computing programs available, the transport parameters are rather well estimated and corroborated by experiment. Mixtures of some noble gases with popular quenchers are considered, with some emphasis on low mass gases. Pure noble gases, for example, argon and xenon, are also presented with single photon detection and medical imaging applications in view, respectively.

1 INTRODUCTION

Particle physics experiments rely heavily on the detection of charged and neutral radiation with gaseous electronics. A suitable gas mixture enclosed within electrodes with an electric field between them permits the detection of charged particles. When ionizing radiation passes through such a system, free charge is liberated in the form of electrons and ions moving under the action of the electric field to the respective electrodes. In high fields, the electrons can be amplified creating a detectable charge signal. The study of the drift and amplification of electrons in a uniform (or non-uniform) electric field has been a fascinating subject of intensive research over the past century. Pioneering work has been done by Townsend and his collaborators which has been well summarized in Ref. 1-17; exhaustive reviews on the progress of the theory and experiments can be found in these references.

For tracking at a high-luminosity hadron collider like LHC, an operational gas mixture has the following requisites: It has to be fast, so that an event can be unambiguously associated to its bunch crossing which leads to a compromise between having a high drift velocity and large primary ionization statistics. The drift velocity would ideally be saturated or have a small variation with modifications in electric and magnetic fields. The mixture needs to be well quenched with no

* mailing address: CERN, Geneva, Switzerland.
e-mail: archana.sharma@cern.ch.

secondary effects like photon feedback and field emission giving a stable gas gain well-separated from the noise of the electronics. Fast ion mobility for quick clearance of positive ions to inhibit space charge effects also helps in having small EXB effects.

Experiments at the upcoming high-luminosity B-f and t-charm factories require a low mass gas mixture and a lot of work has been done in this direction. For low mass gas mixtures, used for detection of low momentum particles by minimizing multiple scattering, it is known that ethane, Isobutane and dimethyl ether (DME) are good quenchers with helium [25-30], which also help increase the number of primary and total ion pairs per cm for a given density.

Clearly, financial constraints also need to be addressed in large gas systems, and a non-flammable, eco-friendly gas mixture is often a prerequisite for safety.

2 STATISTICS OF ELECTRON-ION PAIR PRODUCTION IN A GAS

When an ionizing particle passes through a gas, the free electrons and ions are produced in amounts that depend on the atomic number, density, and ionization potential of the gas, and on the energy and charge of the incident particle. The number of primary electron pairs per cm is called N_p. The created electrons may have sufficient energy to ionize further and create secondary electron-ion pairs. The overall outcome of the two processes is called total ionization; the total number of electron-ion pairs per cm is denoted by N_t. N_p and N_t depend on incident particle charge and velocity, and are characteristic of a given gas or gas mixture. They affect the localization accuracy, and in particular for thin gas gaps in chambers the accuracy is largely affected by the average distance between primary ionization clusters. These numbers, have been measured and computed for a variety of gases [11, 18-24]. Table 1 lists some values for N_p and N_t, along with other general properties. Here E_x and E_i are the excitation and ionization energy, respectively, w_i is the average energy required to produce one electron-ion pair in the gas, and $(dE/dx)_{mip}$ is the most probable energy loss by a minimum ionizing particle. All numbers are for normal temperature and pressure (NTP).

For gas mixtures, a weighted average for N_p and N_t may be computed. A gas density being equal, the number of primaries is larger for gases whose molecules comprise light elements. The numbers given are for minimum ionizing particles; for lower energy particles, the larger ionization density helps improving accuracy.

Table 1: Physical properties of gases at 20°C and 760 Torr.

Gas	Z	A	Density 10^{-3} (g/cm^3)	E_c (eV)	E_i (eV)	w_i (eV)	$[dE/dx]_{mip}$ (keV cm^{-1})	n_p (cm^{-1}) N.T.P	n_t (cm^{-1}) N.T.P.	Radiation Length (m)
He	2	2	0.178	19.8	24.5	41	0.32	4.2	8	745
Ar	18	39.9	1.782	11.6	15.7	26	2.44	23	94	110
Ne	10	20.2	0.90	16.67	21.56	36.3	1.56	12	43	345
Xe	54	131.3	5.86	8.4	12.1	22	6.76	44	307	15
CF_4	42	88	3.93	12.5	15.9	54	7	51	100	92.4
DME	26	46	2.2	6.4	10.0	23.9	3.9	55	160	222
CO_2	22	44	1.98	5.2	13.7	33	3.01	35.5	91	183
CH_4	10	16	0.71	9.8	15.2	28	1.48	25	53	646
C_2H_6	18	30	1.34	8.7	11.7	27	1.15	41	111	340
i-C_4H_{10}	34	58	2.59	6.5	10.6	23	5.93	84	195	169

3 ELECTRON TRANSPORT PROPERTIES

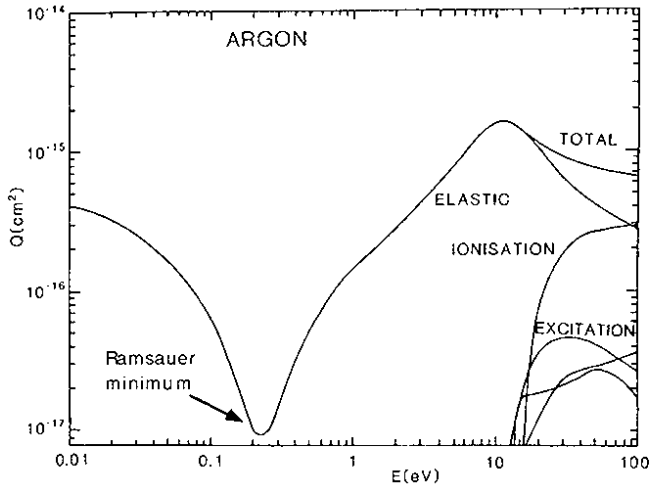

Fig. 1. Cross sections for electron collisions in Argon.

Rigorous treatment of the theory of electron transport has been extensively summarized in the various references quoted [31-33]; here, it is very simply reminded without mathematical detail. In the absence of an electric field, the free electrons in a gas will move randomly, experiencing

collisions with the gas molecules with a Maxwell energy distribution, having an average thermal energy of 3/2 kT (0.04 eV at STP); when an electric field is applied, in addition to their random thermal velocity v, the electrons begin to drift in the field direction with a mean velocity v_d, the average distance covered by the drifting electron swarm per unit time. The energy distribution, Maxwellian in the absence of an electric field, becomes a complicated distribution once the electrons start moving in an electric field, and thus acquiring energy. This energy distribution is even more complicated in the presence of a non-uniform field, for example, resulting from particular detector geometries and/or the presence of magnetic fields requisite for charged particle tracking. When the electrons move in an electric field they may still attain a steady distribution if the energy gained per mean free path is small compared with the electron energy. The momentum transfer per collision is not a constant, especially in excitation and ionization collisions between electrons and atoms, causing a larger energy loss. electrons with energies near the Ramsauer minimum in argon (see Fig. 1), for example (0.23 eV), have long mean free paths, and as a consequence, can gain more energy before experiencing a collision with the surrounding gas. This is taken into account in computing the energy distribution function and has consequences on the gas parameters. The drift velocity is also dependent on pressure, and temperature, and can be modified by the presence of pollutants like water or oxygen (as will be demonstrated in section 5); electronegative pollutants deplete the gas of electrons.

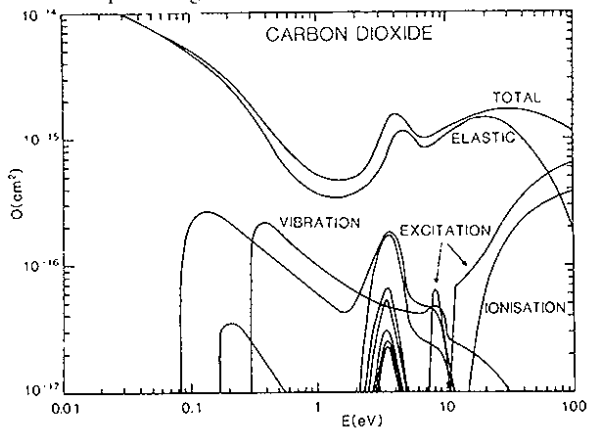

Fig. 2. Electron collision cross sections for carbon dioxide.

Unlike noble gases, polyatomic molecular and organic gases have many other modes of dissipating energy, namely molecular vibrations and rotations. The probabilities of these

mechanical excitations can be as important as those of electronic excitations. The actual mechanism of such interactions is complex and the molecule can be in a final state very different from the ground state of the molecule. The cross-sections of carbon dioxide can be taken as an example, see Fig. 2. It is seen that these collisions are produced at relatively small energies (0.1 to 1 eV) compared to excitation and ionization collisions. The vibrational and rotational excitation cross sections result in the mean fractional energy loss being large and the mean electron energy being low. The mean or "characteristic electron energy" represents the average 'temperature' of the drifting electrons: a gas may be called warm or cold depending upon the average electron energies being above the mean energy limit, in the electric field range considered.

As the electrons are drifting in the electric field, they also disperse symmetrically, thus giving rise to volume diffusion, transverse and longitudinal to the direction of motion. In cold gases like carbon-dioxide for example, the diffusion is small, while drift velocity is low and unsaturated for values of electric fields usual in gas detectors; this implies a non-linear space-time relation. Warm gases, like argon for instance, have a higher diffusion; when mixed with polyatomic/organic gases having vibrational thresholds between 0.1 and 0.5 eV, diffusion is reduced in most cases, while the drift velocity is increased.

Clearly due to the deflection effect exerted by a magnetic field perpendicular to the electric field and the motion of the electron, the electron moves in a helical trajectory resulting in a lowered drift velocity and transverse dispersion. Thus, the arrival time of electrons in a proportional counter, for example, changes and the spread in the drift time increases. The angle which the drifting electron swarm makes with the electric field is defined as the Lorentz angle of the particular gas or gas mixture under consideration. This depends on both the electric field and the magnetic field. It is normally large at small electric fields but falls to smaller values for larger electric fields and is approximately linear with increasing magnetic field. It has been observed that gases with low electron energies have a small Lorentz angle. In case of a small mis-alignment between the electric and magnetic fields, the resulting drift velocity and transverse diffusion will distort the space-time relation at the ends of the drift space in both TPC end-cap multiwire chambers or drift chambers in a magnetic field. Therefore, these effects have to be carefully studied and minimized.

The Boltzmann transport equation expresses the conservation of the number of electrons from the classical Liouvilles theorem for collisions in the absence of amplification, which may be solved numerically knowing the electron distribution function at a point of phase space as a function of time. To solve this equation, this function is expanded in Legendre polynomials, and the terms after the first two contribute to less than 1% and are neglected, giving a set of two coupled differential equations which may be solved exactly.

All calculations presented here are carried out with the MAGBOLTZ computer program for transport parameters developed by S. Biagi [34]. The program was initially developed as a

multiterm Boltzmann expansion allowing the extraction of the absolute cross sections for electron scattering from the experimental data on drift velocity and transverse diffusion. Data from inelastic scattering cross sections are also used. Calculations are carried through to third order Legendre polynomial expansion of the electron distribution function; neglecting higher orders leads to some discrepancy of a few percent in the predicted and measured values of diffusion, especially transverse. These cross sections are then used to compute and predict the transport parameters in various gases and gas mixtures.[1] Figure 3 shows the cross sections DME as an example.

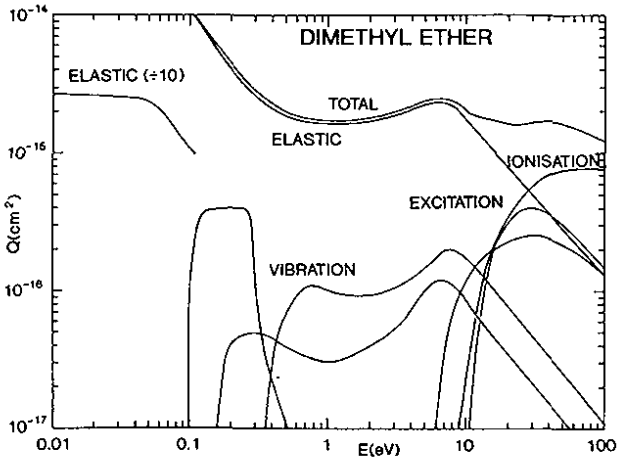

Fig. 3. Electron collision cross sections for dimethylether (DME).

The electron transport overview has been organized as follows: Noble gases Helium, Neon, Argon, and Xenon are mixed with the popular quenchers, namely Methane, Ethane, Isobutane, DME, and Carbon dioxide.[2] Each dataset has been presented in two ranges of the electric field: from 0 to 5000 V/cm on a linear scale, and from 5 to 50000 V/cm on a logarithmic scale. In the first set of transport parameters, the magnetic field is zero. Transport parameters for values of B field 0.5, 1, 2, 3, and 4 Tesla have been computed and presented. Wherever possible, measurements from literature are included. All the plots show the mixtures (noble gas + quencher) varying from pure noble gas to pure quencher in steps of 10% and the scales of each plot in

[1] Different from those which were used as input to the cross sections.
[2] Available at http://wwwcn.cern.ch/writeup/garfield/examples/gas/trans2000.html, and it is being updated regularly.

different gas mixtures have been kept the same to ease comparison. The ambient conditions have been taken to be 20° C and 760 Torr. In this paper, some examples are shown.

3.1 Drift, Diffusion, and Lorentz angles

Figure 4 shows the transport parameters of helium-ethane taken from Ref. 28. The agreement for drift velocity with the computations is rather good while that for diffusion is about 2%.

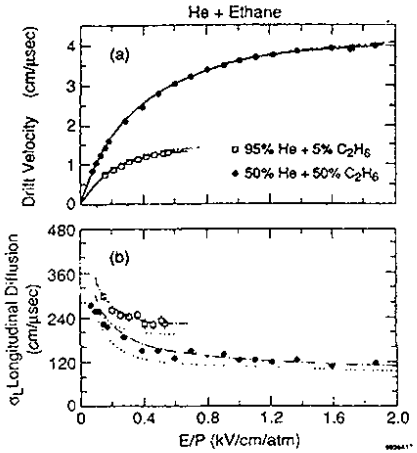

Fig. 4. Measurements and calculation of drift and diffusion for helium-ethane mixtures [28].

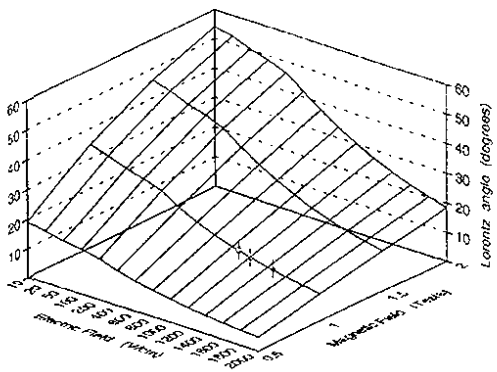

Fig. 5. Lorentz angles for helium-isobutane (90-10) as a function of electric and magnetic field. The points are taken from Ref. 35.

Computations of Lorentz angles for a (90-10) helium-isobutane mixture as a function of electric and magnetic field is shown in Fig. 5. Measurements shown from Ref. 35 agree within 2%, also for a 70-30 gas proportion and the results were consistent with the computations [36]. The diffusion characteristics for Ne-CO_2 mixtures are shown in Fig. 6 taken from Ref. 30. As expected, the results agree within a few percent.

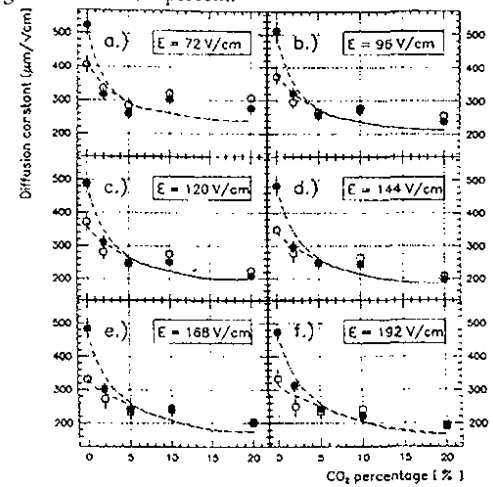

Fig. 6. Measurements (points) and calculations of the longitudinal diffusion constant as a function of the quencher percentage for several values of electric fields for Ne-CO_2 mixtures.

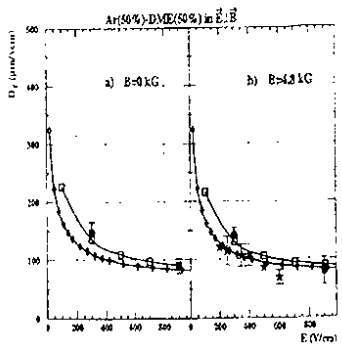

Fig. 7. Measurements and computations of transverse diffusion in Ar-DME (50-50) mixture with and without the presence of a crossed magnetic field. The agreement is within 5%.

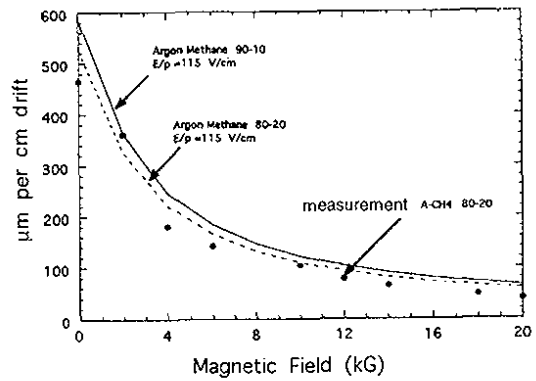

Fig. 8. Measurements [22] and calculations of transverse diffusion in Ar-CH_4 mixtures as a function of magnetic field.

There has been a lot of progress [37] in the field of single photon detection using different kinds of alkali-antimonide photocathodes, the problem being the damage in the presence of usual quencher gases thus necessitating a noble gas, usually argon, as the operational gas. The operation of a proportional gas detector in a pure noble gas has been the subject of many investigations [38]. Figure 9 shows the drift velocity for pure argon taken from Ref. 39 where the curve (computation) is in very good agreement with the calculations.

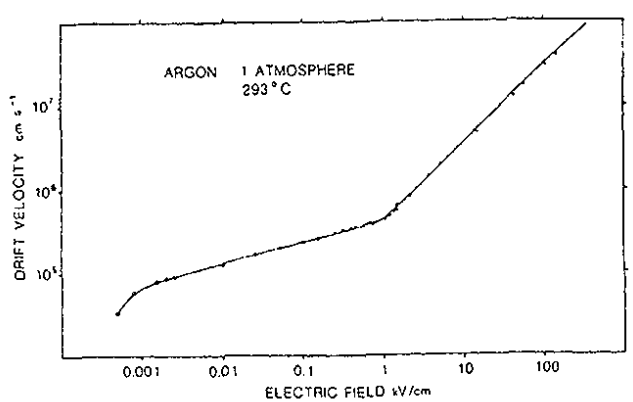

Fig. 9. Drift velocity in pure argon as a function of electric field [39].

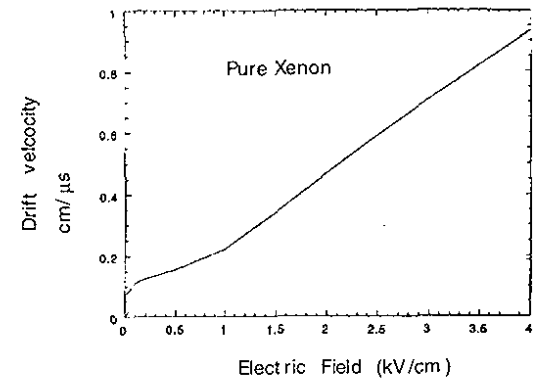

Fig. 10. Drift velocity as a function of electric field and pressure for pure Xenon.

For the purposes of medical imaging, the gas choice is mainly determined by the spatial resolution; CO_2 is generally added to improve the diffusion characteristics. Figure 10 shows the drift velocity for pure Xenon and Fig. 11 some transport parameters for Xe-CO_2 mixtures at STP.

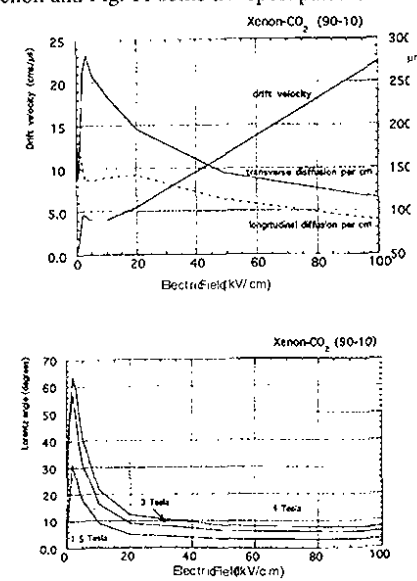

Fig. 11. Some transport parameters of Xe-CO_2 (90-10).

Figure 12 shows the transport parameters for pure DME, used in cases where high accuracy is obtained by exploiting the very low diffusion characteristics and small Lorentz angles of this gas; the measurements are taken from Ref. 40. DME was introduced as a better photon

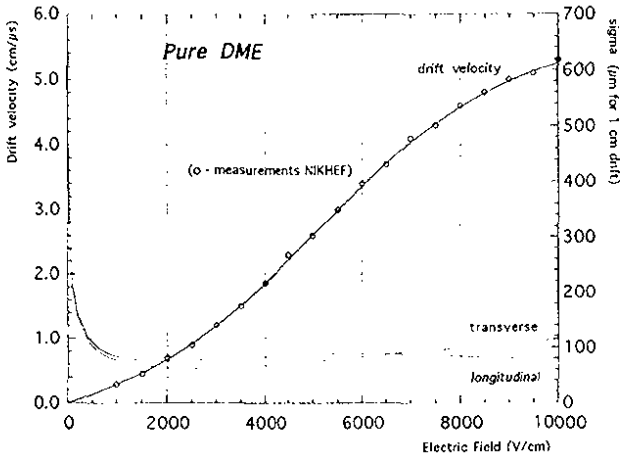

Fig. 12. Transport parameters for pure DME, measurements are taken from Ref. 40.

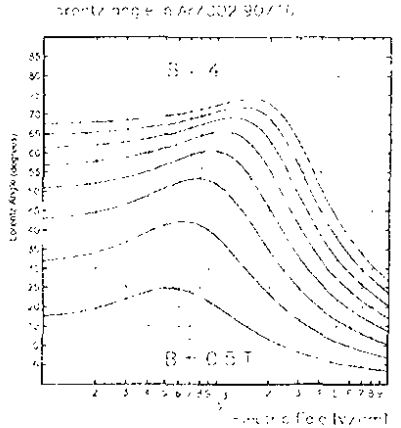

Fig. 13. Lorentz angles in Ar-CO_2 (90-10) from B=0.5 T to 4 T.

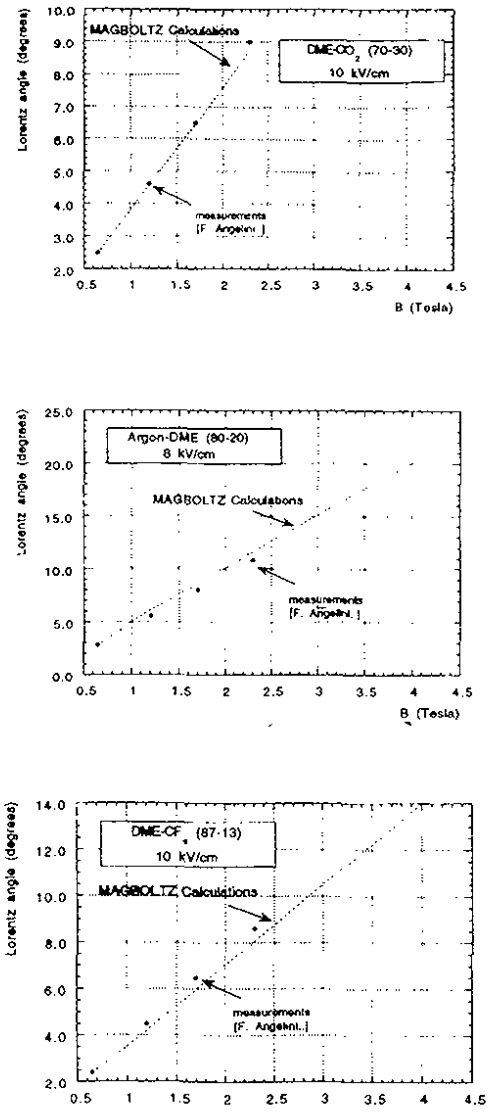

Fig. 14. Measurements of the Lorentz angle for DME based mixtures.

quencher than isobutane; with an absorption edge of ~ 195 nm, it allows for stable operation with convenient gas multplication factors. Consequently, high gains and high rates are possible without rate-induced sparking. Pure DME does not polymerize due to its oxygen-carbon molecular bond, but contaminated DME with freons polymerizes, suggesting high demands on purity and careful choice of materials. Though it is a very cool gas, when mixed with noble gases like neon and argon, the drift velocity increases rapidly. Strangely, one of the fastest gas mixture is made with DME and CO_2, both cool gases. Those for a nonflammable gas mixture of Ar-CO_2 (90-10) are shown in Fig. 13 for a magnetic field ranging from 0.5 to 4 Tesla. Some examples of the calculations and measurements [41] of Lorentz angles for DME and Argon mixtures are shown in Fig. 14.

3.2 Townsend Coefficient

Recently some efforts have been devoted to the measurements of the Townsend coefficient, the mean number of ionizing collisions per unit drift length, in several gas mixtures. Measurements on argon-based mixtures may be found in [42], and Xenon mixtures in Ref. 43. Some measurements of the Townsend coefficient for Helium ethane mixtures are shown in fig. 15, which were done using the experimental setup described in Ref. 42. Comparisons of computations and the experimental data for the Townsend coefficient are exemplified in Fig. 16 for argon-DME mixtures, and in Fig. 17 for a DME-CO_2 mixture.

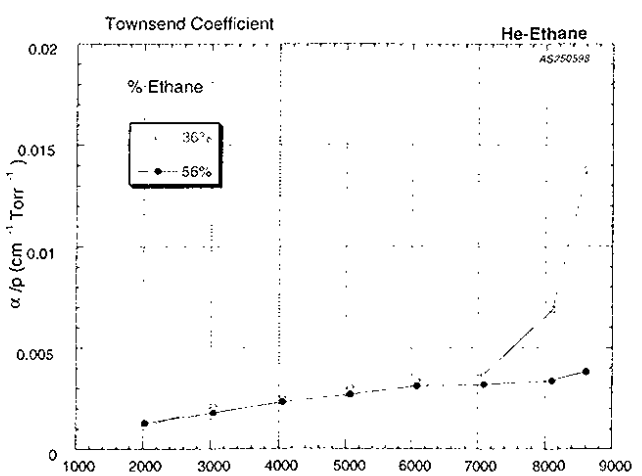

Fig. 15. Measurement of the Townsend coefficient in helium-ethane mixtures.

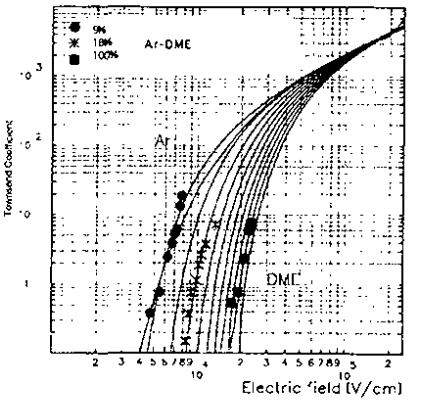

Fig. 16. Computation of the Townsend coefficients and measurements from Ref. 42.

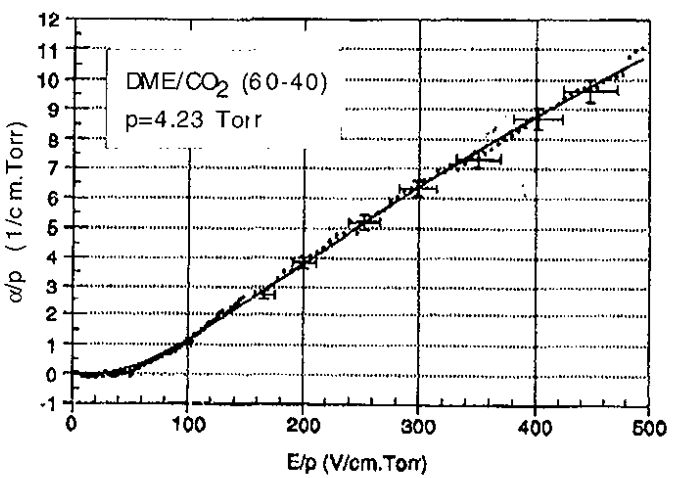

Fig. 17. Calculations and measurements [40] of the Townsend coefficient for DME/CO_2 (60-40).

4 ION TRANSPORT PROPERTIES

The ion mobility is defined as the ratio of drift velocity (v_i) of the ions and the reduced electric field (E/p), in the absence of magnetic field, where E and p are the electric field and pressure,

respectively; it is almost constant up to rather high fields being specific to a particular ion moving in a specific gas. Details may be found in Refs. 15,17 and 24.

Table 2 shows the ion-mobility at atmospheric pressure of some commonly encountered gas molecular ions. In case of two numbers for mobility, the first one comes from the reference on the left, the second from the one on the right.

Gas	Ion	Mobility [cm^2/V.sec]	Reference
Ar	Ar^+	1.00	
Ar	$Methylal^+$	1.51	
iC_4H_{10}	$Methylal^+$	0.55	[38]
Methylal	$Methylal^+$	0.26	[38]
iC_4H_{410}	$iC_4H_{10}^+$	0.614	
Ar	CH_4^+	1.87	[4]
CH_4	CH_4^+	2.26	[38]
Ar	CO_2^+	1.72	
CO_2	CO_2^+	1.09	[38]
C_2H_6	$C_2H_6^+$	1.23,1.24	[38]
CF_4	$C_2H_6^+$	1.04	[2,4]
C_3H_8	$C_3H_8^+$	0.793	[2]
CF_4	CH_4^+	1.06,1.07	[2]
DME	DME$^+$	0.56	[2,4]
CF_4	$C_2H_6^+$	1.04	[3]
CF_4	$C_3H_8^+$	1.04,1.05	[2]
CF_4	$iC_4H_{10}^+$	1.00	[2]
Ar	CH_4^+	2.07,1.87	[2,4]
Ar	$C_2H_6^+$	2.06,2.08	[2,4]
Ar	$C_3H_8^+$	2.08,2.07	[2,4]
Ar	$iC_4H_{10}^+$	2.15,1.56	[2,4]

5 DEPENDENCE OF THE TRANSPORT PARAMETERS ON POLLUTANTS

The presence of pollutants in the operating gas mixture affects the gas detector operation as well. There are two effects: one is the modification of transport parameters and the second is electron loss by capture due to electro-negative pollutants.

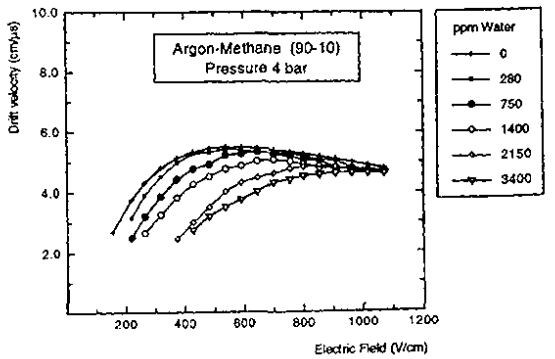

Fig. 18. Effect of the addition of water on the drift velocity in Ar-CH_4 as a function of electric field.

In the case of the addition of water, the static electric dipole moment of the water molecule increases the inelastic scattering cross section for low energy electrons, thus reducing dramatically the drift velocity.

Figure 18 shows measurements of drift velocity [44] exemplifying the effect of the addition of water to an argon-methane (90-10) mixture at ~ 100 V/cm. Adding 1000 ppm of water changes the drift velocity by 20%, while at higher fields the change is negligible. The change is more at higher fields for a noble gas richer mixture. An electron capture (attachment) phenomenon also has a non-negligible electron detachment probability, and the transport parameters may also be sensitive to this electron slowing down mechanism. Incidentally, the first paper by Biagi [31] where the computation program was introduced exemplified the very good agreement between this data and the calculations.

The electron attachment coefficient $C_{en,M}$ may be defined as: $A = P_M \cdot P_{en} \cdot C_{en,M}$,
where A is the attachment rate, P_M and P_{en} are the partial pressures of the gas, and that of the electronegative impurity. The units of $C_{en,M}$ are usually [$bar^{-2}.\mu s^{-1}$], thus if the total drift length in a large detector is measured, say, in 50 μs, an attachment coefficient of 500 represents a loss of 10% in gain per ppm of electronegative pollutant. The gain loss per ppm of oxygen, as a function of the attachment coefficient of several gas mixtures, has been estimated from several measurements [45, 46]. The mean capture length is l estimated and is shown in Table 3, p being the fraction of oxygen in the mixture. For p=0.01 we have for Xenon a lp of 0.8 cm, while for warm gases, this number is quite small. For cold gases however, it is difficult to drift to large distances without electron

capture, as seen from the attachment coefficients; this may impose serious requirements on the purity of the gas.

Table 3

Gas Mixture	Electric Field [V/cm]	lp[cm]
Ar-CH_4 (90-10)	150	5.1 10^{-2}
Ar-CH_4 (90-10)	250	3.4 10^{-2}
Ar-CH_4 (80-20)	100	1.6 10^{-2}
Ar-CH_4 (80-20)	200	2.9 10^{-2}
Ar-CO_2 (80-20)		9.3 10^{-2}
Xe-CH_4 (90-10)	~ 500	7.8 10^{-2}

References

[1] L.B. Loeb, Basic processes of gaseous electronics,(Berkeley: Univeristy of California Press, 1961).

[2] H. Raether, Electron Avalanches and Breakdown in gases, edited by J.D. Craggs and J.M. Meek, (London: Butterworths, 1964).

[3] Electrical Breakdown in gases, edited by J.A. Rees, (London: Macmillan, 1973).

[4] S.C. Curran and J.D. Craggs, Counting tubes, theory and applications (London: Butterworths).

[5] B. Rossi and H. Staub, Ionization chambers and counters. New York: McGraw Hill, 1949.

[6] D.H. Wilkinson, Ionization Chambers and Counters, Cambridge, 1950.

[7] S.A. Korff, Electron and Nuclear counters, New York: Van Nostrand, 1955.

[8] O.C. Allkofer et al., Spark Chambers, Munchen: Theimig, 1969.

[9] P. Rice-Evans, Spark, Streamer, Proportional and Drift Chambers, London: Richelieu, 1974.

[10] G. Charpak, Evolution of the Automatic Spark Chambers, Annu. Rev. Nucl., Sci. 20 (1970) 195.

[11] F. Sauli, Principles of Operation of Multiwire Proportional and Drift Chambers, CERN 77-07 (1977).

[12] F. Sauli, Principles of Operation of Multiwire Proportional and Drift chambers, in Experimental techniques in high energy physics, edited by T. Ferbel (Addison-Wesley, 1987).

[13] G.Charpak and F. Sauli, High Resolution electronic particle detectors, Ann. Rev. Nucl. Sci., 34 (1984) 285.

[14] B. Sadoulet, Fundamental Processes in Drift Chambers. Phys. Scr., 23 (1981) 433.

[15] F. Sauli, High Rate, Position Sensitive Radiation Detectors: Recent developments and Applications in Particle Physics, Medicine and Biology, in the 8th Meeting of the Division of Particles and Fields of the American Physical Society (World Scientific, 1994).

[16] F. Sauli, Gas Detectors: Recent Developments and Applications, CERN-EP/89-71 (1989).

[17] W. Blum and L. Rolandi, Particle detection with drift chambers, edited by F. Bonaudi and C. Fabjan, (Springer-Verlag, 1993).

[18] E.N. Lassestre et al., J. Chem. Phys. 49 (1968) 2382.

[19] S.F. Biagi, Nucl. Instr. and Meth., A283 (1989) 716.

[20] B. Schmidt and K. Martens, HD-PY 92/02 (1992).

[21] R. Bouclier et al., Recent developments of the multidrift tube, Nucl. Intr. and Meth., A283 (1989) 509.

[22] F.F. Reike and W. Prepejchal, Phys. Rev. D, A6 (1972) 1507.

[23] D. Denisov, Nucl. Instr. and Meth., A306 (1991) 200.

[24] G. Schultz, et al., Rev. Appl. Phys., 12 (1977) 67.

[25] A. Sharma and F. Sauli. Operation of drift chambers with low mass gas mixtures, in the 1993 Nuclear Science Symposium and Medical Imaging Conference. 1993. San Francisco, California: IEEE Nuclear and Plasma Science Society.

[26] A. Sharma and F. Sauli, Low mass gas chambers for drift chamber operation, Nucl. Instr. and Meth., A350 (1994) 470.

[27] V. Cindro et al., Nucl. Instr. and Meth., A309 (1991) 411.

[28] J. Va'vra, Nucl. Instr. and Meth., A 324 (1993) 113.

[29] S. Uno et al., KEK Preprint 92-129 (1992).

[30] T. Alber et al., 1994. Nucl. Instr. and Meth., A 349 56.

[31] L.G.H. Huxley and R.W. Crompton, The diffusion and drift of gases, (New York: Wiley, 1974).

[32] V.Palladino and B. Sadoulet, Nucl. Instr. and Meth., 128 (1975) 323.

[33] P. Segur et al., Transport theory and stat. phys., (1986) 705.

[34] S. Biagi, MAGBOLTZ Transport parameters computation program, (Data base for the cross sections of gases, 30 gases) Nucl. Instr. and Meth., A 273 (1988) .

[35] F. Lacava, private communication, 1995 (unpublished).

[36] A. Sharma, Thesis Doctorat No. 2818, University of Geneva, 1996.
[37] A. Breskin et al, Vienna WCC98 and references therein.
[38] F. Sauli, to be published.
[39] S.F. Biagi Nucl. Instr. and Meth., A273 (1988) 533.
[40] D. Kaandorp Eng. Thesis, NIKHEF, 1994.
[41] F. Angeline et al., Nucl. Instr. and Meth., 343 (1994) 441.
[42] A. Sharma and F. Sauli, Nucl. Instr. and Meth., 334 (1993) 420.
[43] H. Sakurai et al.,NASA Preprint 91-114.
[44] I. Lehraus, et al., 84-6, CERN EF 89-8 (1984).
[45] Y. Chiba et al., Nucl. Instr. and Meth., A 269 (1988) 171.
[46] M. Huk et al., HD-PY 87/12 (1987).